EPJ Web of Conferences **20**, 02005 (2012)
DOI: 10.1051/epjconf/20122002005

Kaon photoproduction on the deuteron at Sendai

K. Futatsukawa[1,a], B. Beckford[1], P. Bydžovský[2], T. Fujibayashi[1], Y. Fujii[1], O. Hashimoto[1], Y.C. Han[3], K. Hirose[4], K. Hosomi[1], A. Iguchi[1], T. Ishikawa[4], H. Kanda[1], M. Kaneta[1], D. Kawama[1], T. Kawasaki[1], S. Kiyokawa[1], T. Koike[1], O. Konno[5], K. Maeda[1], N. Maruyama[1], K. Miwa[1], Y. Miyagi[1], S.N. Nakamura[1], A. Sasaki[6], K. Shirotori[1], M. Sotona[2], K. Suzuki[4], T. Tamae[4], H. Tamura[1], N. Terada[1], K. Tsukada[1], and H. Yamazaki[4]

[1] Department of Physics, Tohoku University, Sendai, Miyagi, 980-8578, Japan
[2] Nuclear Physics Institute, 25068 Řež, Czech Republic
[3] School of Nuclear Science and Technology, Lanzhou University, Lanzhou, 730000, China
[4] Laboratory of Nuclear Science, Tohoku University, Sendai, Miyagi, 982-0826, Japan
[5] Department of Electrical Engineering, Ichinoseki National College of Technology, Ichinoseki, Iwate, 021-8511, Japan
[6] Department of Electrical and Electric Engineering, Akita University, Akita, Akita, 010-8502, Japan

Abstract. The photoproduction of K^0 and Λ on the deuteron was measured in order to investigate the $\gamma n \to K^0\Lambda$ reaction process near the threshold (E_γ = 0.8-1.1 GeV). K^0 and Λ events were clearly seen in the $\pi^+\pi^-$ and the $p\pi^-$ invariant mass spectra, respectively. The momentum spectra of the $\gamma d \to K^0 X$ and the $\gamma d \to \Lambda X$ reactions were derived. Additionally, the energy dependence of the integral cross section for the Λ production was also obtained. The K^0 momentum spectra were in agreement with the previous results within statistical errors. The angular distribution of the $\gamma n \to K^0\Lambda$ reaction in the center of mass system was extracted and it had the backward distribution. The total cross section of the $\gamma n \to K^0\Lambda$ reaction, which was estimated by subtracting the contribution of $K^+\Lambda$ process from the Λ production on the deuteron, was almost the same as that of the $\gamma p \to K^+\Lambda$.

1 Introduction

The investigation of the kaon production on the nucleon by the electromagnetic interaction provides invaluable information on the production mechanism, the hadronic structure including missing resonances, and the form factor. Especially, the kaon photoproduction can be described by only four elementary amplitudes. In principle, these amplitudes can be experimentally determined "completely" by measurement of the sixteen observables (differential cross section, three single- and twelve double-polarizations). However, the amplitudes of the $\gamma p \to K^+\Lambda$ reaction with several kinds of observables cannot even be interpreted in spite of theoretical efforts. To overcome the current situation, the experimental data of various set such as for other isospin channels have been eagerly awaited.

The $\gamma n \to K^0\Lambda$ reaction among the six isospin channels plays an important role in investigating the production mechanism due to the following unique features. The production mechanism of the $K\Lambda$ (isospin:I=1/2) production channels is simpler than that of the $K\Sigma$ (I=3/2) because the contributions of Δ^* (I=3/2) resonances are forbidden in the $K\Lambda$ production process. The elementary amplitudes of the $K^0\Lambda$ reaction are constrained by those of the $K^+\Lambda$ because the isospin symmetry are considered. Additionally, the $K^0\Lambda$ reaction involves no charge in the initial and the final states. Then the Born term in the t-channel does not contribute. It might be considered that the angular distribution of the $K^0\Lambda$ production are different from that of the $K^+\Lambda$ [1].

[a] e-mail: kenta-f@lambda.phys.tohoku.ac.jp

2 Experimental apparatus

2.1 Tagged photon beam

This experiment was carried out using a tagged photon beam at Laboratory of Nuclear Science, Tohoku University (LNS-Tohoku). These photons were generated via bremsstrahlung and tagged by the internal tagging system, which is called as STB-Tagger [2].

The energy range of the tagged photons is from 0.8 to 1.1 GeV with the circulating electron beam energy of 1.2 GeV. The intensity was adjusted to about 5-6 mA so that the rate of the summed TagF hits was about 1.5-2.0 MHz. The duty factor was typically modified to 85% in NKS2 from 60% in NKS.

2.2 Neutral Kaon Spectrometer (NKS2)

Based on the success of the previous K^0 experiment using a neutral kaon spectrometer (NKS), we had designed and constructed a new neutral kaon spectrometer (NKS2). Figure 1 shows the schematic view of NKS2. It consists of a dipole magnet, two types of drift chambers (SDC and CDC), inner and outer scintillator hodoscopes (IH and OH), and electron veto scintillation counters (EV).

The dipole magnet with the poles of 1600 mm diameter, which is called 680 Magnet, was installed. The gap size has been expanded to 680 mm. The flux density of the magnetic field is 0.42 T at the center of this magnet with 1000 A. The distribution of the magnetic field for data analysis was calculated by TOSCA program and the flux density was normalized using the peak position of the K^0 invariant mass.

A drift chamber with the cells of the straw type (SDC) was used as a vertex chamber. The typical cell size of SDC was 10.2 mm diameter. SDC was made of three layers and covered the angular range from -150 to 150 degrees. A cylindrical drift chamber (CDC) was located outside SDC to improve the momentum resolution. The shape of the cell is hexagonal and the maximum drift length is about 12 mm. CDC consists of ten layers which are grouped into five groups by two layers. It covers from 200 mm to 800 mm in the radial direction and from -165 to 165 degrees in the angular range. The position resolutions (σ) of SDC and CDC were estimated to be 150 μm and 200 μm, respectively.

TOF counters are two sets of plastic scintillation hodoscopes, i.e. Inner Hodoscope (IH) and Outer Hodoscope (OH). These counters were also used to make the event trigger. IH consists eight plastic scintillators, which are typically 120 mm length and 5 mm thickness, for each left and right arms. These counters surround the target and are arranged from -165 degrees to 165 degrees in the horizontal angle. OH is segmented into 21 pieces for each left and right arms and in each arm has two types, which are horizontal type (OHH) and vertical type (OHV). It was arranged outside of CDC and it covers about π radian. The TOF resolutions against OHV and OHH were 320 ps and 290 ps, respectively.

2.3 Liquid deuterium target

In this experiment, the liquid deuterium target with the cryostat system was used to investigate the $\gamma n \to K^0\Lambda$ reaction. The target was inserted through the central holes of the pole and the yoke of the magnet. The liquid deuterium was stored in the target cell of the cylindrical shape. This cell was placed with its axis parallel to the beam line. Its length was about 30 mm. The target system, which was able to control the liquefaction of deuterium and kept the liquid phase, was adapted to the NKS2 system. During this experiment, the temperature of the liquid deuterium and the pressure of the residual gas were monitored and recorded to estimate the density. The temperature was typically 19 K and the pressure was 50 kPa in the periods of the data taking. The density of the liquid deuterium could be estimated to be 0.174 ± 0.001 μb^{-1} with small ambiguities.

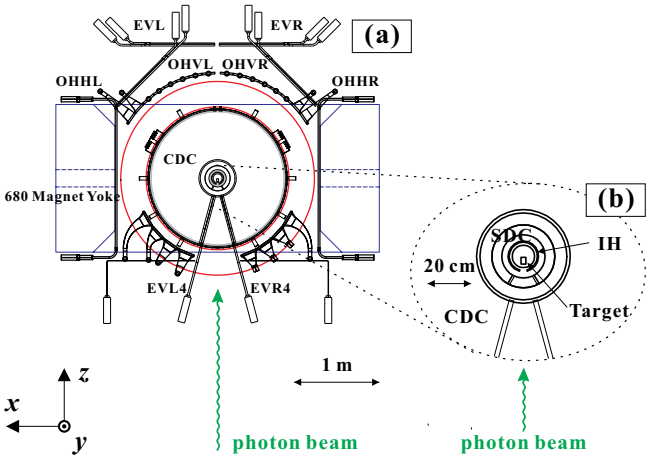

Fig. 1. (a) Schematic view of NKS2. It consists of a dipole magnet (680 Cyclotron Magnet), two types of drift chambers (SDC, CDC), hodoscopes for the time of flight (IH, OH) and electron veto counters (EV). (b) Closeup in the center of NKS2.

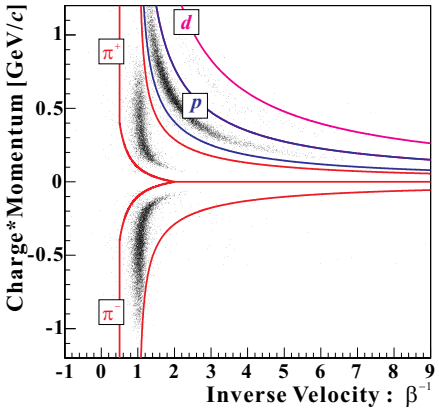

Fig. 2. Correlation between the momentum and the inverse velocity. The sign of the momentum represents the charge of the particle.

3 Analysis

In this analysis, the kind of particles is identified using the correlation between the velocity and the momentum (see Fig. 2). The sign of the longitudinal axis expresses the charge of the particle. A particle in the red and the blue regions was identified by a pion and a proton, respectively.

If more than two tracks can be reconstructed, the vertex point of two tracks is reconstructed. The events with the vertex outside of the target were selected to select K^0 and Λ with longer life time than other hadronic events (decay volume selection). The decay volume selection in detail was described as Ref.[4].

Figure 3(a) and (b) show the invariant mass distributions of $\pi^+\pi^-$ events. The K^0 peak is clearly obtained around 0.5 GeV/c^2. The width in rms by a Gaussian fit is 5.24±0.34 MeV/c^2 for the photon energy (a) from 0.90 to 1.00 GeV and 5.84±0.40 MeV/c^2 (b) from 1.00 to 1.08 GeV. Figure 3(c) and (d) show those of $p\pi^-$ events. The clear peak of Λ mass, whose S/N is more than 10 requiring the cut condition of $|m_{p\pi^-} - m_\Lambda| < 5$ [MeV/c^2] in the high energy region, is obtained around 1.1 GeV/c^2. The resolution in rms is estimated to be 2.06±0.05 MeV/c^2 for the photon energy (c) from 0.90 to 1.00 GeV and 2.13±0.05 MeV/c^2 (d) from 1.00 to 1.08 GeV.

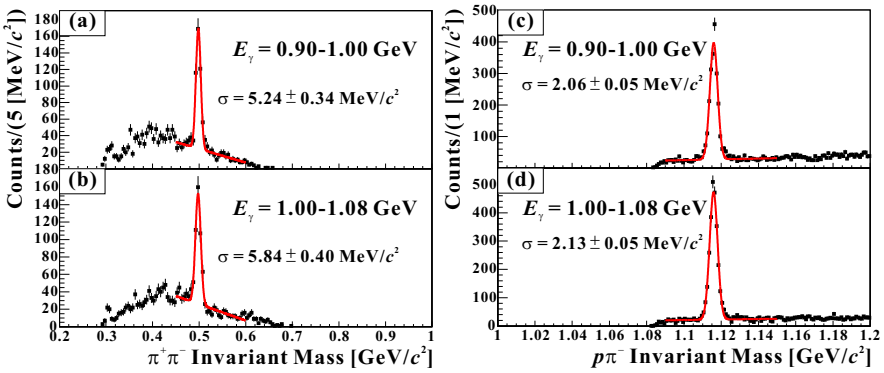

Fig. 3. Invariant mass spectra of $\pi^+\pi^-$ in the photon energy (a) from 0.90 to 0.10 GeV and (b) from 1.00 to 1.08 GeV. Moreover, those of $p\pi^-$ events (c) from 0.90 to 0.10 GeV and (d) from 1.00 to 1.08 GeV are represented.

The acceptances were estimated using the Monte-Carlo simulation based on Geant4. The cross sections of K^0 and Λ were obtained using number of the photons, number of the target, various efficiencies, and the estimated acceptances.

4 Results and Discussion

Momentum spectra for the $\gamma d \to K^0 X$ reaction in the two photon energy regions, 0.90< E_γ ≤1.00 GeV and 1.00< E_γ ≤1.08 GeV, are shown in Fig. 4. These spectra cover extensively in the K^0 production angle than that of NKS [4]. The error bars show the statistical errors in these figures. The systematical uncertainties was estimated to be 11%. The red squares and the black circles in Fig. 4(a) represent the results of NKS and NKS2, respectively. These two results consist within statistical errors. In the high momentum region of $p^{\rm Lab}_{K^0}$ >0.5 GeV/c, the NKS results have the huge errors. On the other hand, it can be confirmed to suppress the statistical errors of this region in NKS2. The lines indicate the theoretical calculations of the $\gamma d \to K^0 \Lambda X$ based on the isobar models by by P. Bydžovský [3]. The solid line predicts those of the Kaon-MAID model (KM)[5,6] and others are those by Saclay-Lyon A (SLA) [7]. Here the ratio of the decay width for $K_1(1270)$, $r_{K_1K\gamma} = -\sqrt{\Gamma_{K_1^0 \to K^0\gamma}/\Gamma_{K_1^+ \to K^+\gamma}}$, has to be taken account as a parameter in the SLA model. The present results in the low energy region are larger than the calculation of KM. The cross section predicted by the SLA model depends greatly on the $r_{K_1K\gamma}$ value in SLA. The K^0 spectra predicted by the SLA model with the $r_{K_1K\gamma}$ value from −1.2 to −1.3 agree well with the experimental data in the absolute value. The shapes of the K^0 spectra in this region are similar to the experimental results. In the higher energy region, the difference between our results and KM is not great in the absolute values except for the distribution of the low momentum ($p^{\rm Lab}_{K^0}$ <0.3 GeV/c) in the angular regions of 0.9< $\cos\theta^{\rm Lab}_{K^0}$ ≤1.0. The inclusive K^0 momentum cannot be compared with the calculation of the $\gamma d \to K^0 \Lambda X$ due to the large contribution of the Σ production in this region. The K^0 spectra with SLA of $r_{K_1K\gamma}$=−1.5 are almost consistent with our results in the regard of not only the absolute but also the shape.

Figure 5(a-d) represents the momentum spectra for the $\gamma d \to \Lambda X$ reaction. The error bars show the statistical errors in these figures. The systematical uncertainties were estimated to be 14%. In addition, the integral cross section for the $\gamma d \to \Lambda X$ reaction was obtained for the first time (see Fig. 5(e)). The integral region of the angular region in the laboratory frame is 0.9< $\cos\theta^{\rm Lab}_{\Lambda}$ ≤1.0. The lines indicate the theoretical calculations adding the $K^0\Lambda$ and the $K^+\Lambda$ processes based on the isobar models.

To show the angular distributions of the elementary $K^0\Lambda$ reaction preferred by the present results, a phenomenological parametrization in the center of mass (c.m.) system was used,

$$\frac{d\sigma}{d\Omega^{CM}} = \sqrt{s - s_0}\,(1 + e_0(s - s_0)) \cdot \left(a_0 + a_1 \cos(\theta^{\rm CM}_{K^0}) + a_2 \cos^2(\theta^{\rm CM}_{K^0})\right). \quad (1)$$

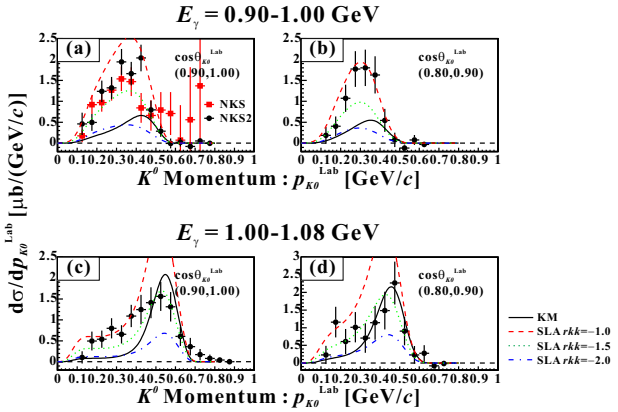

Fig. 4. Momentum spectra for the $\gamma d \to K^0 X$ reaction. The integral regions of the angular range in the laboratory system are displayed in each spectrum.

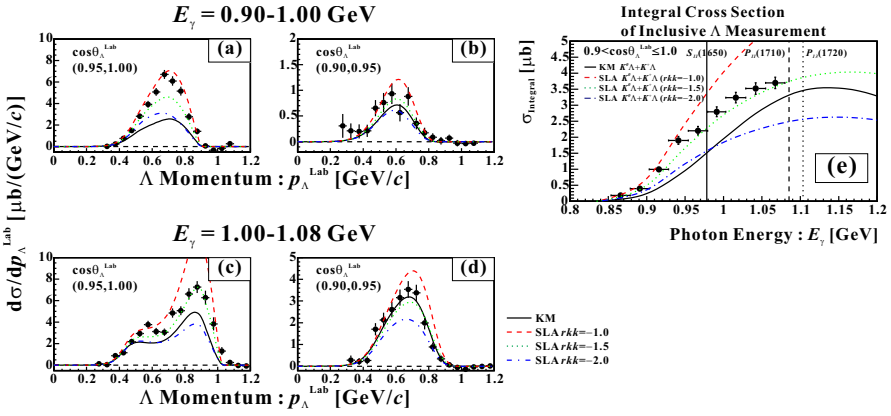

Fig. 5. Momentum spectra (a-d) and integral cross section (e) for the $\gamma d \to K^0 X$ reaction. The angular regions are shown in each figure.

Here $\theta_{K^0}^{CM}$ and s are the K^0 production angle in the c.m. system and the Mandelstam variable (s_0=2.603 GeV^2: $K^0\Lambda$ threshold), respectively. The e_0, a_0, a_1, a_2 and a_3 represent the fitting parameters. The K^0 momentum spectra with the distributions of Eq. (1) were calculated using the Monte-Carlo simulation using the following assumptions,

- the $\gamma n \to K^0\Lambda$ reaction of a quasi-free process,
- Hulthén wave function as Fermi momentum of a neutron in the deuteron.

The simultaneous fit was done for the K^0 momentum spectra of two angular regions in the low energy region (Fig. 4(a) and (b)). Figure 6(a) and (b) shows the best-fit results with the parameters. The angular distribution of the $K^0\Lambda$ production estimating from the present results were compared with that of the $K^+\Lambda$ [8,9]. The $K^0\Lambda$ production has the larger cross section in the backward while the $K^+\Lambda$ shows the slight forward peaking.

The total cross section of the $\gamma n \to K^0\Lambda$ reaction was estimated from the Λ integral cross section on the deuteron, which is generated via the $K^+\Lambda$ and the $K^0\Lambda$ quasi-free processes in the threshold region. We subtracted the $K^+\Lambda$ contributions estimated by the theoretical calculation of KM from the Λ integral cross section. Next, the loss effects of the $K^0\Lambda$ due to out of the acceptance ($\cos\theta_\Lambda^{Lab}$ <0.9) were supplied using the KM model (about 10% at all). Figure 7 shows the comparison of the total cross sections between the $K^0\Lambda$ and the $K^+\Lambda$ reactions [9,10]. The estimated $K^0\Lambda$ total cross section

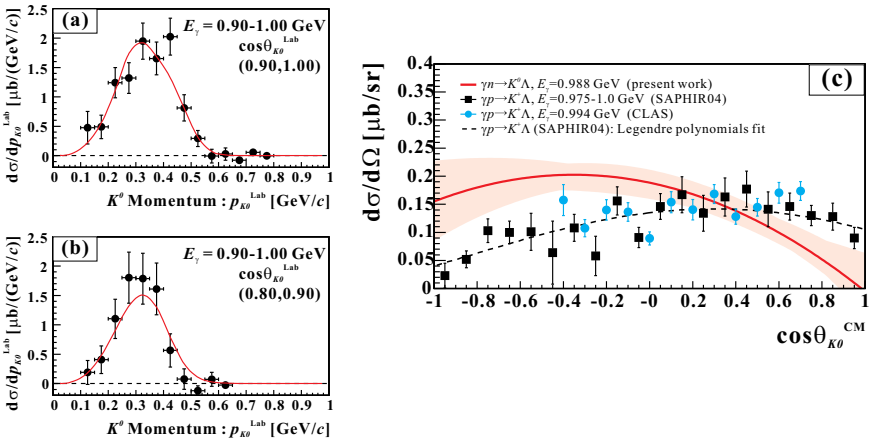

Fig. 6. Fitting results of the K^0 momentum spectra (a)(b) and the estimated $\gamma n \to K^0\Lambda$ angular distribution in the c.m. system (c). Those of the $\gamma p \to K^+\Lambda$ reaction are represented due to the comparison.

was represented as the red circles in the figure. These two data for the $K\Lambda$ productions agree each other in the present energy region reasonably well.

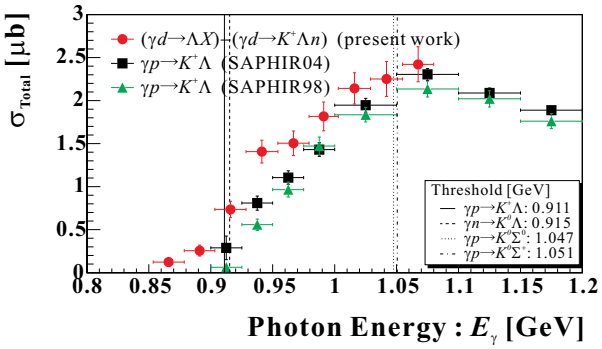

Fig. 7. Comparison of the total cross sections with the $K^+\Lambda$ reaction. The present results (red circles) of the $K^0\Lambda$ production were estimated from the Λ integral cross section.

References

1. X. D. Li, L. E. Wright and C. Bennhold,, Phys. Rev. **C45**, (1992) 2011-2014
2. H. Yamazaki et al., Nucl. Instrum. Meth. **A536**, (2005) 70-78
3. P. Bydžovský, private communication
4. K. Tsukada et al., Phys. Rev. **C78**, (2008) 014001; K. Tsukada et al., Phys. Rev. **C83**, (2011) 039904
5. F. X. Lee, T. Mart, C. Bennhold, and L. E. Wright, Nucl. Phys. **A695**, (2001) 237-272
6. T. Mart and C. Bennhold, Phys. Rev. **C61**, (2000) 012201
7. T. Mizutani, C. Fayard, G. H. Lamot and B. Saghai, Phys. Rev. **C58**, (1998) 75-90
8. R. Bradford et al., Phys. Rev. **C73**, (2006) 035202
9. K. H. Glander et al., Eur. Phys. J. **A19**, (2004) 251-273
10. M. Q. Tran et al., Phys. Lett. **B445**, (1998) 20-26